Absolute de Haas–van Alphen amplitudes and g-factor measurements in Au using the wave-shape-analysis technique*

H. Alles,† R. J. Higgins,‡ and D. H. Lowndes
Department of Physics, University of Oregon, Eugene, Oregon 97403
(Received 25 February 1974)

A technique of de Haas-van Alphen (dHvA) wave-shape analysis is described and used to determine the absolute amplitude of the ⟨111⟩ neck and ⟨110⟩ dog-bone oscillations in pure Au. Only *relative* amplitude and phase measurements of the first and second dHvA harmonics are required. The technique projects out separately both the Lifshitz-Kosevitch dHvA second-harmonic content, and that due to magnetic interaction effects. Measured dHvA *absolute* amplitudes are used to directly determine electronic cyclotron-averaged g factors, with the result that $g_c = 1.04 \pm 0.03$ for the ⟨111⟩ neck orbit and $g_c = 2.04 \pm 0.28$ for the ⟨110⟩ dog-bone orbit. The result for the neck orbit is about 15% less than that obtained by Randles; there have been no previous g-factor determinations for the ⟨110⟩ dog-bone orbit in the noble metals. The problem of experimentally determining the effective demagnetizing factor of a nonellipsoidal sample is discussed.

I. INTRODUCTION

The de Haas–van Alphen (dHvA) effect may be expressed in a form similar[1] to the original Lifschitz-Kosevitch[2] (LK) expression as

$$\tilde{M} = \sum_{r=1}^{\infty} A_r^{\mathrm{LK}} \sin[2\pi r(F/B - \gamma) \mp \pi/4] \ , \qquad (1)$$

where

$$A_r^{\mathrm{LK}} = \frac{DB^{1/2}}{r^{3/2}} \frac{X_r}{\sinh X_r} \cos(\pi r S)\, e^{-\lambda \mu r X_D / B} \ . \qquad (2)$$

F is the dHvA frequency, B is the applied field, γ a phase factor, μ is the electronic reduced cyclotron effective mass, $S = (g\mu/2)$ where g is the electronic cyclotron-averaged g factor, X_D is the Dingle scattering temperature, $X_r = r\lambda\mu T/B$, T is the temperature, $\lambda = 146.9$ kG/K, and D is a geometrical factor proportional to $|d^2A/dk_B^2|^{-1/2}$.

The dHvA wave shape which is observed is frequently distorted from the relatively simple form given by Eq. (1) by the self-modulation process which is known as the magnetic-interaction (MI) effect.[3,4] This wave-shape distortion arises because the dHvA signal is observed as a function of changes in the applied field H, while the electrons respond to the total magnetic induction B, including the effect of the sample's own oscillatory magnetization $\tilde{M}$. MI effects are generally regarded as a problem to be avoided; however, systems of interest frequently display MI effects, and a procedure for accurately calculating the dHvA wave shape in their presence is then required.

In addition, MI effects may be used to great advantage, making it possible to measure the absolute amplitude, $|A_1^{\mathrm{LK}}|$, of the dHvA oscillations without an absolute calibration of the detection apparatus. While earlier absolute-amplitude measurements using the torsion method have been made with sufficient accuracy to check the LK theory to within 10%,[5] the difficulties of either absolute calibration or of accurate harmonic-content measurement have previously limited absolute-amplitude measurements by the modulation technique to about ±30%.[6] The present results demonstrate that under favorable conditions, the modulation technique is capable of absolute-amplitude accuracy comparable to the torsion technique. For a material with a well-known Fermi-surface (FS) geometry, a determination of the absolute amplitude then makes it possible to uniquely determine the numerical value of any *single* unknown factor in $|A_1^{\mathrm{LK}}|$, using Eq. (2). For example, the cosine spin-splitting factor (and from it a set of possible g values) may be determined in this way. This opens up the possibility of g-factor measurements on the larger regions of the FS, where the usual harmonic-content method is inapplicable due to the dominance of MI effects, and the spin-zero method is limited to favorable circumstances where an (accidental) spin zero occurs. It is also possible to measure the scattering temperature X_D (proportional to the cyclotron-averaged electronic scattering rate) in this way, without making the usual logarithmic "Dingle plot" of amplitude vs $1/H$. This can be very useful in magnetic alloy systems where X_D may be field dependent; Dingle plots obscure this field dependence and at best give only a mean Dingle temperature, $\bar{X}_D$, in this case. We shall refer to all such determinations of electronic cyclotron properties, from $|A_1^{\mathrm{LK}}|$, as "absolute" measurements.

II. WAVE-SHAPE-ANALYSIS TECHNIQUES

Explicit relations describing the amplitude and relative phase of the MI contribution to the observed oscillatory magnetization have been derived by Phillips and Gold[4] and by Randles.[6] The first

observable effect of MI is to leave the fundamental ($r=1$) amplitude unchanged but to produce an additional second-harmonic contribution, A_2^{MI}, to the observed dHvA waveform which is phase shifted relative to the LK contribution A_2^{LK}. The existence of this phase shift makes it possible to separate the MI and LK contributions and to determine the amplitude of each.

The field-modulation technique[7] (FMT) is particularly useful for wave-shape measurements because of its "Bessel-function spectrometer" action which makes it possible to enhance weak dHvA harmonic content.[7-9] However, the FMT does introduce both π and $n\pi/2$ phase shifts in the relative phase (in $1/H$) between the various detection harmonics, and these can be difficult to track down. This difficulty may be avoided by using the procedure described below, provided that one uses data taken only at the even detection harmonics $n\omega$ ($n=2, 4, 6, \ldots$) of the modulation frequency ω.[8,12] In addition, in pure samples, skin-depth effects can alter A_2/A_1, leading to a serious error, unless one measures and properly combines signals from quadrature detection phases, and in addition corrects for the actual "modified Bessel function" in the presense of skin effects.[9]

A block of high-resolution dHvA data, consisting of digitized voltages proportional to the oscillatory magnetization and beginning at an arbitrary field value H_0, is Fourier decomposed into sine and cosine components S_r and C_r relative to one edge of the data block. This is done for each of the first

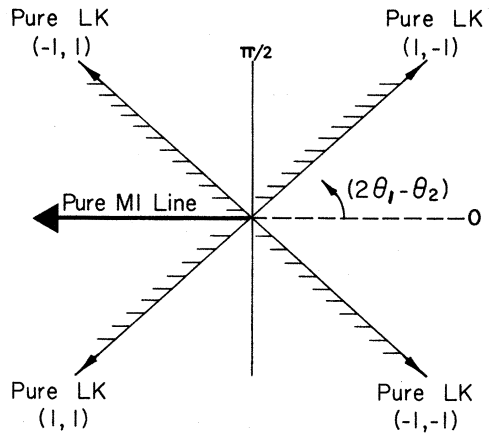

FIG. 1. Illustrating all possible ranges of values for the observable phase parameter $\theta=2\theta_1-\theta_2$ (see text). In general θ lies between the appropriate pure-LK and pure-MI limiting values, i.e., to the left of the appropriate vector representing the pure-LK limit and labeled by the indices (p,q). The notation (p,q) is used to label the various possible pure-LK limiting values, where $p=-1$ $(+1)$ for an extremal orbit for which the extremal area is a maximum (minimum) with respect to k_H, while $q=-1$ $(+1)$ for $\cos(2\pi S)$ less (greater) than zero.

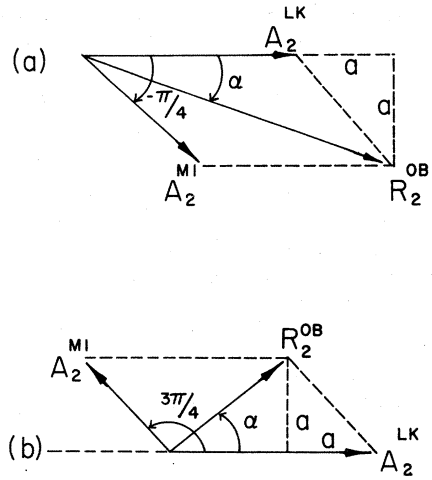

FIG. 2. Phasor diagram decomposition of the observed $r=2$ resultant amplitude, in terms of its LK and MI components: (a) for $\cos(2\pi S)>0$ $(q=+1)$; (b) for $\cos(2\pi S)<0$ $(q=-1)$. For either case, $A_2^{MI}=\sqrt{2}\,R_2^{OB}\sin\alpha=\kappa(1-N)\times(R_1^{OB})^2/2$, while $A_2^{LK}=R_2^{OB}(\cos\alpha-q\sin\alpha)$, where α is the angle by which the observed $r=2$ resultant, R_2^{OB}, deviates from the pure-LK limit.

two dHvA harmonics in the observed oscillatory voltage signal $[V^{OB}=(S_r^2+C_r^2)^{1/2},\ r=1,2]$ so that the directly measured quantities are resultant harmonic voltage amplitudes V^{OB} and harmonic phase angles θ_r. The phase angle θ_r for each observed harmonic amplitude, relative to H_0, is defined as

$$\theta_r=\tan^{-1}(S_r/C_r). \tag{3}$$

Although θ_r depends on H_0, the quantity $2\theta_1-\theta_2$ is independent of the (arbitrary) choice of H_0.[8,9] Furthermore, it can be shown[10] (i) that the value of $2\theta_1-\theta_2$ for the *observed voltage signal* can differ from $2\theta_1-\theta_2$ for the *oscillatory magnetization* only by $n\pi$ and (ii) that the resultant possible ambiguity of π in the value of $2\theta_1-\theta_2$ for the magnetization can always be uniquely resolved using the observed H or T dependence of $2\theta_1-\theta_2$. Since $A_2^{LK}/A_2^{MI}\propto H^{5/2}/T$, increasing H (or decreasing T) will tend to make A_2^{LK} dominant, and θ will approach its pure-LK limiting value. Figure 1 summarizes the range of all possible values for $2\theta_1-\theta_2$. The magnitude of the *relative* phase angle,

$$\theta\equiv|2\theta_1-\theta_2|, \tag{4}$$

is always within either the range $\pi/4\le\theta\le\pi$ or the range $3\pi/4\le\theta\le\pi$, depending on the sign of the spin-splitting factor, $\cos(2\pi S)$, with the value $\theta=\pi$ corresponding to the pure-MI limit.

Figure 2 is a phasor diagram illustrating the effect of MI on the resultant $r=2$ magnetization amplitude R_2^{OB} and phase angle θ_2. Each term (LK or MI) contributing to R_2^{OB} is represented by a phasor whose length and phase angle are the magnitude and

dHvA phase of this term (with increasing dHvA phase plotted counter clockwise from the positive x axis). Zero phase angle corresponds to a pure-LK $r=2$ signal A_2^{LK}. The phase of A_2^{LK} depends on the sign of the $r=2$ spin-splitting factor $\cos(2\pi S)$, so that there are the two possible phasor diagrams shown in Fig. 2.

Since the observed value of θ_2^{OB} can deviate from the pure-LK limiting value only because of an appreciable MI component, it is convenient to define

$$\alpha \equiv \theta_2^{OB} - \theta_2^{LK} \tag{5}$$

the angle by which θ_2^{OB}, the observed value of θ_2, deviates from the (known) pure-LK limiting value. With this definition then

$$(2\theta_1 - \theta_2)^{OB} = (2\theta_1 - \theta_2)^{LK} - \alpha. \tag{6}$$

Using Fig. 1, R_2^{OB} may be projected into its LK and MI components,

$$A_2^{LK} = R_2^{OB}(\cos\alpha \pm \sin\alpha), \tag{7}$$

$$A_2^{MI} = \sqrt{2}\, R_2^{OB} \sin\alpha = \tfrac{1}{2}\kappa(1-N)(R_1^{OB})^2, \tag{8}$$

with $\kappa = 8\pi^2 F/H^2$, and N is the demagnetizing factor of the sample. A discussion of this extension of the Phillips and Gold expressions to include demagnetization is given in Appendix A. The positive (negative) sign in (7) is for $\cos(2\pi S)$ negative (positive). The three observable voltage amplitudes are then GR_1^{OB}, GA_2^{LK}, and GA_2^{MI}, where G is the detection-system gain. G is dependent upon the detection harmonic number n, and is proportional to the modified Bessel function of order n, J_n.[9] The ratio of these Bessel-function multipliers, for dHvA frequencies F and $2F$, can be determined by a separate calibration.[8,9] Thus, three amplitude ratios can then be formed, any pair of which are independent, with the (unknown) absolute system gain G canceling out in these ratios. For example, for any detection harmonic n,

$$\frac{J_n(x)GA_2^{MI}}{J_n(2x)GR_1^{OB}} = \frac{\sqrt{2}R_2^{OB}\sin\alpha}{R_1^{OB}} = \tfrac{1}{2}\kappa(1-N)R_1^{OB}$$
$$= \tfrac{1}{2}\kappa(1-N)|A_1^{LK}|, \tag{9}$$

so that, if N is known, it is only necessary to measure the relative amplitudes and phases of the resultant first and second dHvA harmonics in order to find the absolute dHvA fundamental amplitude $|A_1^{LK}|$.

III. EXPERIMENTAL

We have made precise dHvA wave-shape measurements on the ⟨111⟩ neck and ⟨110⟩ dog-bone orbits in pure Au samples, in order to verify the above quantitative expressions for MI and to evaluate the g factor for these two orbits using two different and independent parts of the total information available from wave-shape analysis. The g factor for the neck orbit near ⟨111⟩ was measured earlier by Randles, and dHvA spin-splitting zeros have been observed for the neck oscillations ~25° away from ⟨111⟩. However, no g values have been reported for the dog-bone orbit and the only determination for an orbit in the belly region of the Fermi surface is the value $g=2.35\pm0.05$, from a spin-splitting zero 71.6° from ⟨100⟩ in the (110) plane.[11]

The two samples used in these experiments were single-crystal rectangular prisms of Au which were grown by the Bridgman technique, spark cut from the ingot, heavily etched to remove surface damage and annealed before use to remove deep damage due to spark cutting. The long axes of the two samples were along ⟨111⟩ and ⟨110⟩, respectively; the samples were mounted in a small-angle rotator and oriented parallel to the applied field within 0.05°. The sample dimensions were $2.60\times0.89\times0.97$ mm (⟨111⟩) and $2.84\times1.05\times0.75$ mm (⟨110⟩). The field-modulation technique was employed in an automated data-taking system centered on a laboratory computer and designed to make precise wave-shape measurements.[12,13] The data used in obtaining the results described below is the average of data obtained from the 4ω, 6ω, and 8ω detection channels. The amplitudes were computed by an iterative procedure combining precise Fourier analysis with the successive subtraction of largest Fourier components, so as to reveal weak harmonic amplitudes (Appendix C).

IV. RESULTS

A. ⟨111⟩ neck orbit

The ⟨111⟩ neck orbit in Au is ideal for a test of wave-shape-analysis techniques. The absolute amplitude $|A_1^{LK}|$ is sufficiently large that appreciable MI harmonic content is generated, yet the LK second harmonic is also large, making it possible to verify the relations discussed above. The first-harmonic resultant (voltage) amplitude R_1^{OB}, the ratio of first- and second-harmonic resultant amplitudes R_2^{OB}/R_1^{OB}, and the relative phase θ were measured over a magnetic field range of 24 to 49 kG. The results of these measurements are given in Fig. 3. The phase shift α of the $r=2$ resultant exhibits the expected behavior, approaching zero (LK contribution dominating) at high fields. The comparable scatter in both R_2^{OB}/R_1^{OB} and $(1-N)A_1^{LK}$, in spite of the relatively small values of α [see Eq. (8)], is a measure of the precision with which the phase measurements can be made.

The scattering temperature X_D may be determined from the slope (vs $1/H$) of each of three semi-independent functions which can be formed from the data of Table I. Using Eqs. (2), (7), and (9), each of the following expressions is a linear function of $1/H$, with slope equal to $-\lambda\mu X_D$:

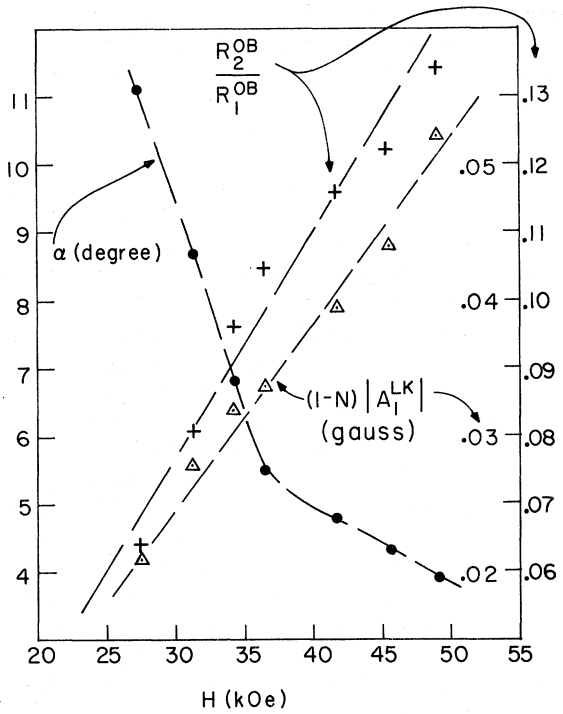

FIG. 3. Measured values of R_2^{OB}/R_1^{OB} and $(1-N)A_1^{LK}$ (right-hand ordinates) and of α [Eq. (6), left-hand ordinate] vs magnetic field (in kOe) for the ⟨111⟩ neck orbit in Au at $T=1.24$ K. The theoretical limiting value of α is 0° (corresponding to no $r=2$ MI contribution), at high H and low T.

$$\ln(R_1^{OB}\sinh X_1/H^{1/2}X_1), \tag{10}$$

$$\ln\left(\frac{R_2^{OB}(\cos\alpha-\sin\alpha)}{R_1^{OB}}\frac{\sqrt{2}\sinh X_2}{\sinh X_1}\right), \tag{11}$$

$$\ln\left(\frac{2}{\kappa}\frac{\sqrt{2}R_2^{OB}\sin\alpha}{R_1^{OB}}\frac{\sinh X_1}{H^{1/2}X_1}\right). \tag{12}$$

Expression (10) is just the conventional "Dingle plot" used to find the scattering temperature from the fundamental ($r=1$) dHvA amplitude. Note, however, that reductions in amplitude due to skin effects cancel in expressions (11) and (12). Expression (11) uses the ratio of the LK projection of the observed second-harmonic amplitude to the observed first-harmonic amplitude. The gain of the experimental detection system cancels in this ratio. The function in Eq. (11) is equal to $e^{-\lambda\mu X_D/H}|\cos\times(2\pi S)/\cos(\pi S)|$, and so (11) may also be used to evaluate the spin-splitting factor [Eq. (2)], once X_D is known.

Expression (12) utilizes the *absolute* LK fundamental dHvA amplitude determined from the MI contribution to the observed second harmonic. Again, the system gain cancels in this ratio so that $|A_1^{LK}|$ can be determined without an absolute calibration of the experimental apparatus. The three values of X_D, determined from expressions (10)–(12) (see Fig. 4) agree rather well, being 0.22 ± 0.003, $0.225+0.05$, and 0.18 ± 0.04, respectively. The consistency of these values obtained from three independent ratios demonstrates the accuracy of the projection technique, even when the MI component is a small fraction of A_2. (The shift α from the LK phase is only $\lesssim 10°$.)

1. *g factor from projected LK harmonic ratio.* Using Eqs. (11) and (2), the ratio of the $r=1$ and $r=2$ LK spin-splitting factors can be evaluated as

$$\rho=\frac{\cos(2\pi S)}{\cos(\pi S)} = e^{\lambda\mu X_D/H}\frac{R_2^{OB}(\cos\alpha-\sin\alpha)}{R_1^{OB}}\frac{\sqrt{2}\sinh X_2}{\sinh X_1}. \tag{13}$$

Taking $\mu=0.28$,[14] and using the measured value of $X_D=0.22$, ρ was evaluated for each field value from

TABLE 1. Harmonic amplitudes and phases and derived information for the ⟨111⟩ neck orbit. Left: relative harmonic amplitudes and phases. Center: ratio of cosine spin-splitting factors, derived from the LK component of R_2/R_1. Right: cosine spin-splitting factor, derived from the absolute amplitude obtained by a projection of the MI component of R_2/R_1.

H (kOe)	R_2^{OB}/R_1^{OB}	α (deg)	LK harmonic ratio $\rho=\lvert\cos(2\pi S)/\cos(\pi S)\rvert$ $\cos\alpha+\sin\alpha$	$\cos\alpha-\sin\alpha$	Abs. ampl. projection $(1-N)_{eff}\cos(\pi S)$
27.55	0.064	11.1	1.00	0.649	0.488
31.30	0.081	8.7	0.95	0.678	0.505
34.73	0.096	6.8	0.92	0.706	0.496
37.93	0.105	5.5	0.86	0.693	0.464
41.70	0.116	4.8	0.83	0.686	0.482
45.32	0.122	4.3	0.80	0.663	0.490
49.32	0.134	3.5	0.78	0.671	0.528
			monotonic trend	0.678 ± 0.018 average $g_N=1.04\pm0.03$	0.488 ± 0.015 average

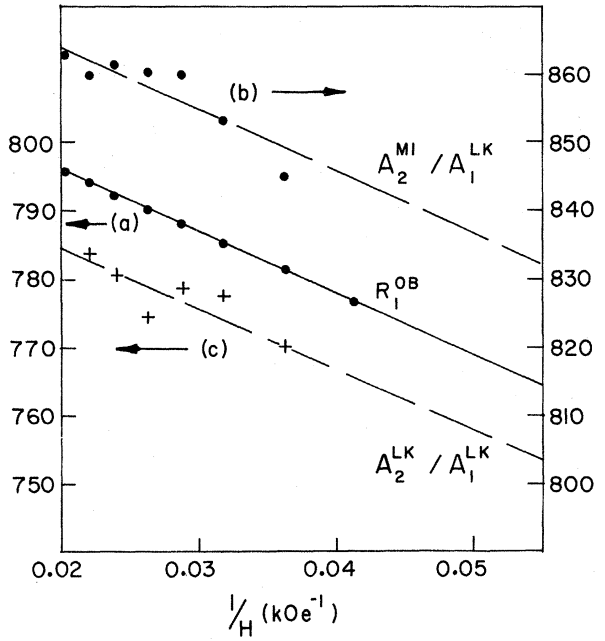

FIG. 4. "Dingle plots" for three different parameters formed from the ⟨111⟩ neck-orbit data of Table I (ordinates in arbitrary units) vs 1/H: (a) Eq. (10); (b) Eq. (11); (c) Eq. (12). The dashed lines shown are drawn parallel to the solid line, which is the best (least-squares) fit to (a).

27 to 49 kG (Table I). The average value is $\bar{\rho} = 0.678 \pm 0.018$. The proper choice of sign in Eq. (7) [minus is shown in Eq. (13)] is demonstrated in Table I. Since the left side of (13) is field independent, the measured combination on the right should also be field independent. Note that although this method determines the sign of $\cos(2\pi S)$, it does not remove any of the ambiguity $(n \pm S)$ in the determination of g from the ratio of cosines. Following the discussion of Randles[6] and using absolute-phase measurements[15] to reduce the ambiguity yields a value of the ⟨111⟩ neck-orbit g factor of $g_N = 1.04 \pm 0.03$. This is about 15% *lower* than Randles value of $g_N = 1.22 \pm 0.12$.[6]

2. *g factor from projected absolute amplitudes.* The g factor can also be obtained from absolute amplitudes measured by the projection technique [Eq. (9) and Fig. 2], which could be especially useful for large orbits where the LK harmonic amplitude is overwhelmed by MI, or where the (accidental) spin-zero technique is inapplicable. Comparing the measured A_1^{LK} [Eq. (9)] with the same quantity calculated from Eq. (2) yields a value for $\cos(\pi S)$. The principle uncertainty in (2) is the curvature factor d^2A/dk_B^2 contained in D. The principal uncertainty in (9) is the demagnetizing factor. As a test of the experimental technique (particularly the measurement of phases) we choose the neck orbit, for which the g factor has been determined independently above. This test reveals a previously unsuspected skin-depth effect via the demagnetizing factor.

It is convenient to write the quantity of interest by combining Eqs. (2) and (9):

$$(1-N)_{eff}\cos(\pi S) = \frac{2}{\kappa}\frac{\sqrt{2}R_2\sin\alpha}{R_1^{OB}}\left(\frac{A_1^{LK}}{\cos(\pi S)}\right)^{-1}.$$

The first factor on the right comes from the measurement. The second factor may be calculated from Eq. (1), using the value of X determined above. For the curvature factor in (1) we use $(d^2A/dk_B^2)^{-1/2} = 0.26$, obtained from an inversion fit of Fermi-surface data.[14] An independent check using neck-orbit data only (Appendix B) gives 0.260, so that this factor is reliable to 1%. The results, shown in the right column of Table I, show no systematic field dependence, and are self-consistent to within ±3%, in spite of the fact that the phase shift α from which they are obtained is small ($\lesssim 11°$) and systematically decreasing with increasing H. This demonstrates the reliability of the projection technique. However, a comparison of g values from the two methods requires an accurate value for the demagnetization factor.

For a sample with a non-second-order surface, the internal demagnetizing field is nonuniform, so that the demagnetizing factor also depends upon position, $N = N(r)$. Joseph and Schlomann[16] have described a method for calculating the demagnetizing field, and $N(r)$, for uniformly magnetized samples which have the shape of a rectangular prism. Their results show directly that the demagnetizing field, and $N(r)$, can be highly nonuniform. In samples with dimensional ratios of order 2:1:1, N varies from ~0.5 (near the long-axis end faces which are perpendicular to H) to ~0.1 (near the center of the sample). An example is shown in Fig. 5. A volume average of this calcu-

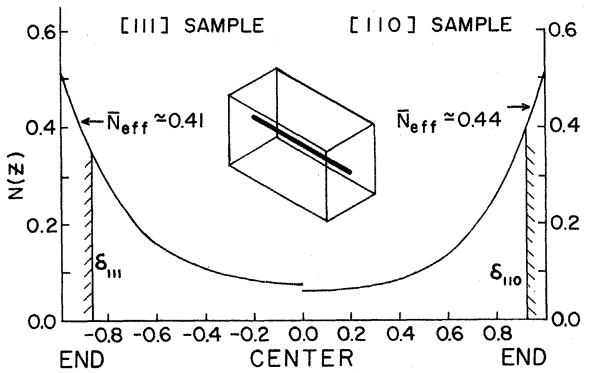

FIG. 5. Spatially varying demagnetization factor calculated using the method of Ref. 16 for a sample with the dimensions used. Also shown are the skin depths calculated at $f = 500$ Hz, using measured magnetoresistance (Ref. 17).

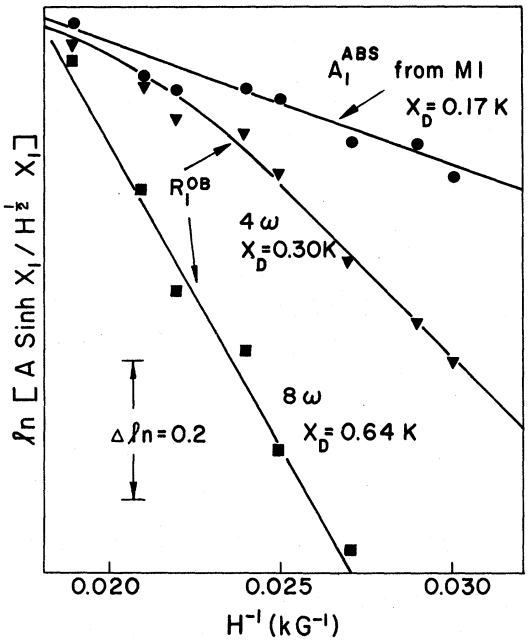

FIG. 6. "Dingle plot" of $\ln[(1-N)\ |A_1^{LK}|\ \sinh X/X \times H^{1/2})]$ vs $1/H$ [see Eq. (14)] for the ⟨110⟩ dog-bone orbit in Au at $T=1.24$ K. The slope corresponds to $X_D=0.17 \pm 0.03$ K. Also shown are conventional amplitudes R_1^{OB} measured in the 4ω and 8ω detection channels. The various apparent X_D values are due to skin-depth effects (see text).

lation for the [111] sample yields $N_{eff}=0.14$, or using Table I, $\cos(\pi S)=0.51$. This is to be compared with a value $\cos(\pi S)=0.89$ from the LK harmonic ratio (above). The difference amounts to 40%, far outside the limits of error of the measurement (±5% for the MI measurement in Table I, and ±3% for the LK measurement in Table I). Our interpretation requires a discussion of skin effects present in the measurement.

3. *Skin effects and absolute amplitudes.* Skin effects are made rather severe by the relatively low magnetoresistance of Au, which reaches a saturation value $\Delta\rho/\rho$ of 4 at [111] and of only 1 at [110]. A computation of the skin depth δ at a frequency of 800 Hz (8ω) yields 0.17 mm at [111] and 0.11 mm at [110]. As a result, the effective demagnetizing factor is not the average, but is weighted towards the surfaces and end regions of the sample, where n is largest. An estimate of N within one skin depth yields $\overline{N}_{eff}=0.41$ (see Fig. 6), which, together with Table I, gives $\cos(\pi S)=0.83$, less than 4% away from the value obtained from the LK harmonic ratio. This good agreement is probably fortuitous, because of the complicated spatial variation of N, but it does demonstrate that the origin of the discrepancy lies in skin effects entering through the demagnetization factor. This demonstrates the need in future g-factor measurements with the absolute-amplitude technique either for the use of ellipsoidal samples, or of long thin samples (N_e small) and lower detection frequencies to minimize uncertainty in $(1-N_e)$. We therefore restrict our attention in the balance of this paper to one example where the *direction* of the uncertainty leads to no error in the result. (See Sec. IV B).

Note that averaging data from the 4ω, 6ω, and 8ω detection-frequency channels does not introduce a substantial error in the results due to skin effects. The volume actually sampled drops out of the amplitude *ratios* used, and the demagnetization factor is frequency insensitive when only the surface layer is sampled, as in this case. To check this, amplitude ratios A_2/A_1 were computed separately as a function of detection frequency. The values differed typically by only ±3% when the frequency changed by a factor of 2. Note, however, that it is essential *not* to use the usual Bessel functions of the field-modulation technique to obtain these numbers when in the skin-depth region. As reported earlier[9] for Cu-Fe, the dependence of A_r upon modulation amplitude differs significantly from simple J_n proportionality. In evaluating A_2/A_1, the *measured* ratios of modified Bessel functions[9] were used, i.e.,

$$A_2/A_1=(S_2/S_1)_n[J_n^{eff}(\lambda_1)/J_n^{eff}(\lambda_2)].$$

Here, $(S_2/S_1)_n$ is the ratio of measured signal levels of second- and first-harmonic Fourier components in the $n\omega$ detection channel, and the ratio of *effective* Bessel functions is *measured* using a doubled modulation field[9]:

$$J_n^{eff}(\lambda_1)/J_n^{eff}(\lambda_2)=J_n^{eff}(\lambda_1)/J_n^{eff}(2\lambda_1)=S_1(\lambda_1)/S_1(2\lambda_1).$$

These ratios are significantly different from the ratios of J_n. For example, using [111] neck-orbit data at 1.24 K and 45 kG, with a modulation level $\lambda=4.6$:

	$n=4$	$n=6$	$n=8$
$[J_n^{eff}(\lambda_1)/J_n^{eff}(\lambda_2)]_{meas}$:	7.12	2.19	30.92
$(A_2/A_1)_{meas}$:	0.1202	0.1265	0.1215
$[J_n(\lambda_1)/J_n(\lambda_2)]_{calc}$:	0.76	1.76	29.7

The good agreement (±3%) between A_2/A_1 values in the different channels is evidence that this technique gives reliable results even when skin effects modify the Bessel functions substantially (up to a factor of 10) from J_n. Note that the modifications are not largest at the higher frequencies but rather the reverse. The modification is largest in the 4ω and 6ω channels because the principal effect of skin effects is to shift the location of the Bessel zeros.

TABLE II. Results of $r=1$ and $r=2$ wave-shape-analysis measurements on the ⟨110⟩ dog-bone orbit in Au at $T=1.24$ K.

H (kOe)	$\frac{R_2^{OB}}{R_1^{OB}}$	$\frac{2R_2^{OB}}{\kappa R_1^{OB}} = (1-N)A_1^{LK}$ (G)	$\left(\frac{A_1^{LK}}{\cos(\pi S)}\right)_{calc}$ [a]	$\cos(\pi S)$ [b]
33.02	0.0406	0.00580	0.00958	1.01
34.84	0.0497	0.00790	0.01285	1.03
37.06	0.0577	0.01037	0.01767	0.98
39.32	0.0705	0.01427	0.02350	1.01
42.02	0.0835	0.01930	0.03168	1.02
45.03	0.0949	0.02519	0.04227	0.99
48.61	0.1118	0.03458	0.05672	1.02

[a] $X_D = 0.17 \pm 0.03$; $|d^2A/dk_B^2|^{-1/2} = 0.26$ (Ref. 14).
[b] $\cos(\pi S)$ obtained from the ratio of $(1-N)A_1^{LK}$ to $[A_1^{LK}/\cos(\pi S)]_{calc}$. A value of $N_{eff} = 0.40$ was used (see text).

B. ⟨110⟩ dog-bone orbit

dHvA wave-shape-analysis measurements were also made on the ⟨110⟩ dog-bone orbit in Au, using another sample. This orbit is ordinarily somewhat difficult for precise amplitude measurements because of the small magnetoresistance, which makes skin-depth problems more noticeable. However, by using only amplitude ratios R_2^{OB}/R_1^{OB}, amplitude reductions due to the reduced volume seen as a result of skin effects cancel. There was no observable A_2^{LK} for the dog bone at 1.24 K for $33 \le H \le 53$ kOe, the value of α being $45° \pm 2°$ for all field values. Thus, all of the observed dHvA second-harmonic signal is due to MI, and the analysis does not require the projection technique used for the ⟨111⟩ neck orbit, though the lack of LK harmonic content (in the range of field available to us) does mean that the total information available from wave-shape-analysis techniques is less.

Our results for R_2^{OB}/R_1^{OB} vs H are given in Table II. Using Eq. (9), the measured value of $(1-N) \times |A_1^{LK}|$ is just $(2/\kappa)(R_2^{OB}/R_1^{OB})$ and is also given in Table II. The scattering temperature X_D may then be obtained from the absolute amplitudes by plotting

$$\ln\left(\frac{2}{\kappa}\frac{R_2^{OB}}{R_1^{OB}}\frac{\sinh X}{XH^{1/2}}\right) = \ln\left((1-N)|A_1^{LK}|\frac{\sinh X}{XH^{1/2}}\right) \qquad (14)$$

vs $1/H$, as shown in Fig. 6. The slope gives $X_D = 0.17 \pm 0.03$ K. We note that a determination of X_D by the usual method from the observed amplitudes R_1^{OB} leads to a serious error due to the field-dependent skin depth in this case. Also shown in Fig. 6 are plots of R_1^{OB} as seen in the 4ω and 8ω detection channel. The values of X_D (0.30 and 0.64 K) differ by factors of 2 and 4, respectively, from the value obtained from A_1^{LK} by the absolute-amplitude method. The difference is due to the decreasing volume sampled by R_1^{OB} as $1/H$ increases. This effect is more serious in higher detection frequencies, owing to the smaller skin depth, and more serious at [110] than [111], owing to the smaller magnetoresistance (see Sec. IV A 3) at [110]. As a check, we note that no such effects were observed at [111] (see Fig. 4), and the X_D value from A_1^{ABS} is consistent both with the measured residual resistance ratio and the X_D value at [111] (both samples were from the same crystal) but inconsistent if the X_D values from R_1^{OB} are used. Note that the effective volume drops out in the ratio used to extract A_1^{ABS}.

Using this value of X_D, $[A_1^{LK}/\cos(\pi S)]_{calc}$ may be calculated and compared with $(1-N)A_1^{LK}$, as shown in Table II. In calculating A_1^{LK} we use a value of $(d^2A/dk_B^2)^{-1/2} = 0.26$ obtained from Ref. 14 which is uncertain by at most a few percent (see Appendix B).

The principal uncertainty comes in estimating $1-N$. The neck-orbit measurements of $\cos(\pi S)$ demonstrated that N is dominated by the surface region. In the absence of measureable LK second harmonic as a check, we use as a first approximation the *effective* value of N determined in Sec. IV A 2. This value must be adjusted for the slightly different dimension of the [111] and [110] samples. Adjusting N_e by the ratios of N values calculated by the method of Ref. 16 gives $N_e = 0.40$. Using this value (Table II) gives a mean value $\cos(\pi S) = 1.01 \pm 0.10$, where the quoted error is principally the effect of the ± 0.03 K uncertainty in X_D. This gives $g_c = 2.04 \pm 0.28$, assuming the most probable argument ($S=1$) for the cosine function. It should be noted that the relatively large resultant uncertainty in g_c is due primarily to the *insensitivity* of the cosine function itself to small changes in g_c (or S) in the neighborhood of $S=1$, via the effect of the *small* uncertainty in X_D on the *calculated* value of A_1^{LK}, but is *not* due to any large uncertainties in the *measured* A_1^{LK} amplitudes, as demonstrated by the small scatter in the last column of Table II.

Our use of N_{eff} obtained from [111] does not lead to an increased uncertainty in $\cos(\pi S)$ in spite of the factor of 4 smaller magnetoresistance at [110]. Referring to Fig. 5 (right half), an improved estimate of N_{eff} may be obtained by scaling the measured N_{eff} [111] by the ratio of calculated values averaged over 1 skin depth. The result is $N_{eff}[110] = 0.47$, giving $\cos(\pi S) = 1.14 \pm 0.10$. Although the precise value of $N_{eff}[110]$ is uncertain, the direction of the change due to skin depth is quite clear, and pushes $\cos(\pi S)$ to values larger than 1, which is impossible.

V. SUMMARY

(i). A measurement of g from LK harmonic content for the neck orbit at [111] in Au yields $g_N = 1.04 \pm 0.03$, a value 15% lower than an earlier measurement.[6]

(ii). A test of g measurements from absolute amplitudes determined from the magnetic-interaction component of R_2/R_1 yields a value of $\cos(\pi S)$ of 0.51, which is 40% lower than the value determined from the LK harmonic content. The difference is interpreted as a skin-depth effect entering through the demagnetizing factor N, which is spatially varying in parallelipiped samples. Viewed as an effective N_{eff}, the value of N_{eff} is quite consistent with calculated $N(r)$ averaged over the skin depth.

(iii). The determination of scattering temperatures X_D for the [111] neck orbit has been made by three independent methods: the conventional amplitude method (R_1^{OB}), the LK harmonic ratio (A_2^{LK}/A_1^{LK}), and the absolute amplitude A_1^{LK} determined from A_2^{MI}/A_1^{LK}. The internal consistency of the results demonstrates the reliability of the projection technique.

(iv). A determination of X_D for the [110] dog bone by two independent methods yields values which are not consistent. Use of the conventional amplitude method (R_1^{OB}) yields values which vary with detection frequency, and differ by more than a factor of 2 with the value obtained from the absolute amplitudes projected from R_2/R_1. The difference is shown to be a skin-depth effect, which is severe at [110] due to the low magnetoresistance.

(v). The g value for the [110] dog-bone orbit has been measured from the absolute amplitudes A_1^{LK} measured by projecting the magnetic interaction component of R_2/R_1. The results give $\cos(\pi S) = 1.01 \pm 0.10$, or $g_c = 2.04 \pm 0.28$. Corrections due to the smaller skin depth at [110] are shown to be unimportant, owing to the fortunate accident that the cosine has an upper bound of 1.0.

ACKNOWLEDGMENTS

Portions of this manuscript were prepared while one of us (R. J. H.) was a resident visitor at Bell Laboratories. We would like to thank our colleagues at that institution for their hospitality. In particular, we thank W. A. Reed for a helpful discussion of magnetoresistance.

APPENDIX A: MODIFICATIONS TO THE OSCILLATORY MAGNETIZATION (INCLUDING MAGNETIC INTERACTIONS) IN THE PRESENCE OF A DEMAGNETIZING FIELD

In order to make accurate dHvA amplitude measurements in nonspherical samples, it is important to correctly include demagnetization effects. First, since the usual derivation of demagnetization assumes a linear relation between B and M, it is not obvious that the same result emerges when M is oscillatory in B. Second, with the primary change just $M \to (1-N)M$, then the second-harmonic content induced by magnetic interaction might be assumed proportional to

$$A_2^{MI} \propto \kappa[(1-N)A_1]^2 \propto (1-N)^2.$$

It will be shown that, instead, demagnetization makes $\kappa \to (1-N)\kappa$, in which case

$$A_2^{MI} \propto (1-N),$$

i.e., *linear* rather than quadratic in $(1-N)$.

The first point follows by assuming that a given value of M creates a demagnetizing B_d and H_d:

$$B_d = (1-N)4\pi M, \quad H_d = -N4\pi M.$$

The demagnetizing factor N may be viewed as purely *geometric*, originating in a mapping of lines of field under a coordinate transformation. Therefore, the *value* of N will *not* depend on *how* M varies with B.[18] Following Kittel[19] we assume the electron sees the sum of the applied and induced B fields:

$$B = B_0 + B_d;$$

but $B_0 = H_0$ (field applied outside the medium). It follows that $B = H + 4\pi(1-N)M$, and therefore

$$M = \sum_r A_r \sin\{2\pi F/[H_0 + (1-N)4\pi M] \mp \pi/4 - r\phi\}, \tag{A1}$$

proving the first point.

The second point follows from the above by analogy with the Phillips and Gold[4] expansion technique. For $4\pi(1-N)M/H \ll 1$, we can write (A1) as

$$M = \sum_r A_r \sin[r(x - \kappa' M) \mp \pi/4], \tag{A2}$$

where

$$x = 2\pi F/H - \phi \quad \text{and} \quad \kappa' = (1-N)8\pi^2 F/H^2.$$

κ' is identical with Phillips and Gold's κ with the additional factor of $(1-N)$. An expansion of (A2) then yields

$$A_2^{MI} \propto \kappa' A_1^2 = (1-N)\kappa A_1^2, \tag{A3}$$

proving the second point.

APPENDIX B: OBTAINING d^2A/dk_B^2 FROM ROTATION CURVES

Although values of extremal areas are known with very high precision (~0.01%) in metals such as Au, and first-derivative quantities such as m^*/m_0 with reasonable (~1%) precision, there are no direct measurements of d^2A/dk_B^2, a quantity which must be known in order to calculate g factors from A_1^{LK} [see Eq. (2)]. A fit to the area and m^* data yields parameters from which d^2A/dk_B^2 can be calculated. However, in attempting to find a best fit over the entire FS, accuracy at a given point may be sacrificed. Since errors may increase in the second derivative, it is useful as a check to find a method which uses only data in the region of interest. The method described below uses information from rotation curves ($d^2A/d\theta^2$) for the orbit of interest to get d^2A/dk_B^2. It is perhaps well known but we include it here for completeness since it has apparently not appeared previously in print.

1. *Ellipsoid or hyperboloid of revolution*

A straightforward expression of $A(\theta)$ and $A(B)$ in terms of the parameters of a second-order surface of revolution when B is along the axis of symmetry yields

$$\frac{d^2A}{dk_B^2} = 2\pi\left[1 - \left(\frac{1}{A_0}\right)\frac{d^2A}{d\theta^2}\right], \quad A_0 = A(\theta = 0).$$

The neck orbit $A(\theta)$ is well fit as a hyperboloid of revolution, and accurate neck data exist.[20] For comparison, d^2A/dk_B^2 values have been computed from an over-all fit by Bossachi *et al.*[14] The results are as follows:

	$(d^2A/dk_B^2)^{-1/2}$
Hyperboloidal fit to neck $A(\theta)$:	0.260
Derivative of over-all FS fit:	0.26

2. *General second-order surface*

Here two rotation curves in perpendicular directions (1, 2) are required. The result, for H along one of the principal axes, is

$$\frac{d^2A}{dk_B^2} = 2\pi\left\{\left[1 - \left(\frac{1}{A_0}\right)\frac{d^2A}{d\theta^2}\right]_1\left[1 - \left(\frac{1}{A_0}\right)\frac{d^2A}{d\theta^2}\right]_2\right\}^{1/2}.$$

Fitting ⟨110⟩ dog-bone rotation curves[14] in two orthogonal planes with the above expressions yields a curvature value which may be compared with that derived from a derivative of the over-all FS fit[14]:

	$(d^2A/dk_B^2)^{-1/2}$
Second-order fit to dog-bone $A(\theta)$:	0.232
Derivative of over-all FS fit:	0.26

The agreement for neck data is excellent. The agreement for the dog bone is adequate as a check, given that the orbit is not a second-order surface.

APPENDIX C: FOURIER DECOMPOSITION OF PRECISE AMPLITUDES AND PHASES

The precise determination of harmonic amplitudes and phases was made possible (even though the dHvA harmonic content amounts to only a few percent in typical cases) by exploiting the capabilities of the field-modulation technique, and by careful attention to spectral-analysis techniques. A brief account is given here; more details are given elsewhere.[8]

Modulation spectrometry. The resolution of the A/D converter limits the precision with which two Fourier components can be compared. With weak harmonics, this would be a serious problem were it not for the fact that the Bessel-function response of the field-modulation technique allows an enhancement of harmonic amplitudes. Detecting at the eighth harmonic, for example, allows an enhancement of A_2/A_1 by a factor of 25 or more. As a result, the first and second harmonics in the measured signal at 8ω may be made of roughly equal magnitude, and A/D resolution is not a limiting factor.

The window. The field sweep is adjusted so as to give about 8 dHvA cycles within a 256-point sample or window. The modulation amplitude is adjusted continuously to cover a constant fraction of a cycle. With this small number of dHvA cycles, the exponential variation of amplitude within a window is kept negligible. With a small number of cycles per window, the number of samples per cycle of the higher harmonics was kept large, allowing precise amplitude determination in the presence of noise.

Fourier decomposition. As a consequence of the small window, sidebands of the fundamental in a conventional Fourier transform (FT) would completely obscure small-harmonic amplitudes. Window weighting can reduce or eliminate sidebands, but at the expense of spectral resolution. Triangular window weighting was used to reduce sidebands, and a combined Fourier-analysis–least-squares procedure was developed to *remove* the dominant Fourier components iteratively so that successively smaller components at other frequencies were revealed. A Cooley-Tukey fast Fourier transform was *not* used, since a high-resolution conventional FT allows far superior determination of frequencies, amplitudes, and especially phases.[21] The iterative procedure was as follows:

1. Determine precise window frequency of fundamental (high-precision FT).
2. Determine precise amplitude of largest FT peak, and subtract that signal from original data.
3. Fourier analyze new signal (data minus domi-

nant Fourier component).

4. Find the next largest peak in FT and subtract it from signal.

5. Continue with succeeding peaks.

These amplitudes were used as starting values in the next iteration:

1. Subtract all but the largest Fourier component from the data. With precise FT, determine its amplitude and phase precisely.

2. Subtract all but the second largest, and determine its amplitude and phase precisely.

3. Continue until all peak amplitudes done.

4. Subtract everything, and calculate residual "noise," used as a measure of the error.

This iterative procedure was fast enough to be carried out in a minute or two while the magnet was being swept to the next window. It proved remarkably successful. In tests with generated data, Fourier components a factor of 100 smaller than a dominant component (and far smaller than its sidebands) could be recovered with an accuracy of 1%. Accurate phase measurements are more difficult, especially in the presence of noise, because the calculated phase depends critically on knowing the frequency very well. As long as one harmonic was strong enough to serve as a frequency reference, phase measurements accurate to 1 deg were possible.

---

*Research conducted at the University of Oregon with the support of the National Science Foundation and the Research Corporation.

†Present address: Bell Laboratories, Murray Hill, NJ 07974.

‡Resident Visitor 1972–1973, Bell Laboratories, Murray Hill, NJ 07974.

[1]See, for example, the article by A. V. Gold, in *Solid State Physics, Vol.* 1: *Electrons in Metals*, edited by J. F. Cochran and R. R. Haering (Gordon and Breach, New York, 1968), pp. 39–126.

[2]I. M. Lifshitz and A. M. Kosevitch, Zh. Eksp. Teor. Fiz. 29, 730 (1953) [Sov. Phys.-JETP 2, 636 (1956)].

[3]D. Shoenberg, Philos. Trans. R. Soc. Lond. A 255, 85 (1962); A. B. Pippard, Proc. R. Soc. A 272, 192 (1963).

[4]R. A. Phillips and A. V. Gold, Phys. Rev. 178, 932 (1969).

[5]D. Shoenberg and J. Vanderkooy, J. Low Temp. Phys. 2, 484 (1970).

[6]D. L. Randles, Proc. R. Soc. A 331, 85 (1972).

[7]A. Goldstein, S. J. Williamson, and S. Foner, Rev. Sci. Instrum. 36, 1356 (1965); L. R. Windmiller and J. B. Ketterson, Rev. Sci. Instrum. 39, 1672 (1968); R. W. Stark and L. R. Windmiller, Cryogenics 8, 272 (1968).

[8]H. G. Alles, thesis (University of Oregon, 1972) (unpublished); available from University Microfilms, Ann Arbor, Mich.

[9]H. G. Alles and R. J. Higgins, Phys. Rev. B 9, 158 (1974).

[10]D. H. Lowndes, R. J. Higgins, and H. G. Alles, Advances in Physics (to be published); D. H. Lowndes, lecture notes on dHvA wave-shape analysis (unpublished).

[11]G. W. Crabtree, L. R. Windmiller, and J. B. Ketterson, Bull. Am. Phys. Soc. 19, 63 (1974).

[12]H. G. Alles and R. H. Higgins, Rev. Sci. Instrum. 44, 1646 (1973).

[13]H. G. Alles and R. J. Higgins, Rev. Sci. Instrum. (to be published).

[14]B. Bosacchi, J. B. Ketterson, and L. R. Windmiller, Phys. Rev. B 4, 1197 (1971).

[15]P. T. Coleridge and I. M. Templeton, J. Phys. F 2, 643 (1972).

[16]R. I. Joseph and E. Schlomann, J. Appl. Phys. 36, 1579 (1965).

[17]Yu. P. Gaidukov, Zh. Eksp. Teor. Fiz. 37, 1281 (1959). [Sov. Phys. JETP 10, 913 (1960)].

[18]This argument is strictly true only for bodies of second-order shape; in other cases the value of N depends upon the susceptibility. See, for example, H. Zijlstra, *Experimental Methods in Magnetism* (North-Holland, Amsterdam, 1967), Vol. 2, p. 69ff. However, the restricted region $\kappa A_1 < 1$ in which the Phillips and Gold treatment is valid corresponds to the limit $\chi = 0$ in the demagnetization calculation, in which case N is once again a purely geometric quantity.

[19]C. Kittel, Phys. Rev. Lett. 10, 339 (1963).

[20]A. S. Joseph, A. C. Thorsen, and F. A. Blum, Phys. Rev. 140, A 2046 (1965).

[21]R. J. Higgins, Am. J. Phys. (to be published).